

Final Report

High Background Ozone Events in the Houston-Galveston-Brazoria Area: Causes, Effects, and Case Studies of Central American Fires

AQRP Project 16-008

Prepared for:

Elena McDonald-Buller

Texas Air Quality Research Program
The University of Texas at Austin

Prepared by:

Yuxuan Wang (Principal Investigator)
Robert Talbot (Co-principal Investigator)

Department of Earth and Atmospheric Sciences
University of Houston
Houston, TX77204

October 2017

QA Requirements: Audits of Data Quality: 10% Required

Acknowledgement

The preparation was funded by a grant from the Texas Air Quality Research Program (AQRP) at The University of Texas at Austin through the Texas Emission Reduction Program (TERP) and the Texas Commission on Environmental Quality (TCEQ). The findings, opinions and conclusions are the work of the author(s) and do not necessarily represent findings, opinions, or conclusions of the AQRP or the TCEQ.

Executive Summary

A significant fraction of surface ozone in Texas comes from regional background originating from outside the state. Background ozone is particularly variable over the Houston-Galveston-Brazoria (HGB) region due to two main factors: meteorology and out-of-state emissions. This project first estimated and quantitatively separated the effects of a number of meteorological events on peak ozone and background ozone in HGB. With regard to out-of-state emissions, the second part of the project focused on fire emissions from Central America, a large fire region globally of unique importance to Texas air quality whose impact on Texas background ozone has not been quantified previously.

Long-term meteorological and ozone data were analyzed to identify the days of five meteorological events (heat wave, stagnation, thunderstorm, cold front, and post front) and three high ozone events (exceedance, top 15% peak ozone, and top 15% background ozone) in the HGB region during the ozone season (April - October) of 2000 – 2015. Changes in peak ozone and background ozone distributions were compared for each event, except for heat wave because of its extremely uneven distribution. The effects of meteorological events on peak and background ozone were ranked by changes in median ozone during the event days as compared to the non-event days. These analyses led to the following major findings:

1. High background ozone days often have high peak ozone; for example, the top 15% background ozone days have 30 ppbv higher peak ozone than the other 85% of days and coincide with 55.5% of ozone exceedances.
2. Background ozone plays a more important role than local ozone in relative contribution to ozone exceedance at HGB. About 62% of exceedance days would have been avoided during the study period if background ozone had been reduced by 30%. The same fractional reduction of local ozone would have avoided only 40% of exceedance days.
3. The ranking of meteorological events according to their effects on HGB peak ozone is: stagnation > post front > cold front > thunderstorm, and the ranking based on background ozone effects is: post front > cold front > stagnation > thunderstorm. Only thunderstorm

shows a decreasing effect on peak and background ozone; other meteorological events are all associated with higher levels of peak and background ozone.

4. Stagnation has the largest effect on both peak ozone and background ozone at HGB, causing an increase in the median of peak ozone by 26 ppbv and background ozone by 16 ppbv. The associated effects are largest in spring, with 50% co-occurrence with exceedance, followed by 40% during fall.
5. Post front increases ozone in all seasons, with the median enhancement of 11 ppbv for peak ozone and 12 ppbv for background ozone. Cold front has a comparatively smaller effect. Both events are interconnected and co-occur with 15% of high ozone days.

The second part identified the days when Central American fires were transported to HGB and quantified those fire impacts on HGB background ozone during April and May of 2000 to 2015 using back trajectory analysis and GEOS-Chem model simulations. Observational and modeling analyses of Central American fire impacts led to the following major findings:

6. Strong evidence is found consistently from ground measurements, satellite observations, and modeling that Central American fires cause significant ozone enhancements at HGB on episodic bases during springtime.
7. The average number of days when HGB experience significant influences from long-range transport of Central American fire plumes is estimated of 2.1 days per month during April and May, with large temporal variability.
8. Two independent methods give qualitatively consistent estimates of ozone enhancements at HGB due to Central American fires in springtime: 5.67 ± 1.00 ppbv from the back trajectory method and 8.8 ± 1.6 ppbv from the GEOS-Chem passive tracer simulation.
9. Both MOPITT and MODIS satellite instruments detect significant enhancements of CO column densities and AOD, respectively, along the transport route from Central America fire regions to HGB during the GEOS-Chem identified fire-impact days, leading support to the modeling methodology.

Table of Content

1. Introduction.....	7
2. Methods	8
2.1 Study Area.....	8
2.2 Ozone Data and Meteorological Data.....	9
2.3 Satellite Data.....	10
2.4 High ozone events and meteorological Events.....	11
2.5 Background ozone contribution	12
2.6 Back Trajectory.....	13
2.7 GEOS-Chem model	14
2.8 GEOS-Chem-based selection of fire-impact days	15
3. Quality Assurance/Quality Control Procedures.....	16
3.1 Quality of secondary data.....	16
3.2 Quality of GEOS-Chem modeling.....	16
4. Results	17
4.1 Ozone Time Series	17
4.2 Events time series.....	19
4.3 Ozone distribution changes during events	22
4.4 Co-occurrence of events.....	26
4.5 Contribution of background ozone to peak ozone by event	28
4.6 Back trajectory analysis	31
4.7 GEOS-Chem simulation of fire cases.....	32
4.8 Passive tracer simulation	34
4.9 Satellite observations	35
5. Conclusion	36
6. Recommendation for Future Work.....	38
7. References.....	40

List of Figures

- Figure 1.** Research area: the HGB region (red box), NARR reanalysis data points (*), CAMS sites (red dots), and airports (blue dots) with thunderstorm information. 8
- Figure 2.** Weather map sample of the WPC surface analysis valid for 04/04/2014 at 12 UTC. 10
- Figure 3.** Two boxes are defined over the main fire emission sources in Central America. 13
- Figure 4.** Source regions of the six passive tracers in GEOS-Chem: US (excluding Texas; green), Texas (excluding Houston; brown), Houston (yellow), Mexico (pink), Gulf of Mexico (light blue), and the rest of Central America (RCA; dark blue). The mask file is at a resolution of $0.5^{\circ} \times 0.5^{\circ}$. 15
- Figure 5.** Year (left column) and monthly (right column) time series of average peak MDA8 (lower row) and background (upper row) ozone mixing ratio. 18
- Figure 6.** Year time series of mean peak ozone during exceedance days (top left), mean peak ozone during the top 15% peak ozone days (top right), mean background ozone during the top 15% background ozone days (bottom left), and mean peak ozone during the top 15% background ozone days (bottom right). 19
- Figure 7.** Year (left) and monthly (right) time series of exceedance days. 20
- Figure 8.** Year (left) and monthly (right) time series of heat wave days. 20
- Figure 9.** Year (left) and monthly (right) time series of stagnation days. 21
- Figure 10.** Year (left) and monthly (right) time series of thunderstorm days. 21
- Figure 11.** Year (left) and monthly (right) time series of cold front days. 22
- Figure 12.** Probability density curves of peak (left) and background (right) ozone mixing ratio during stagnation days (red lines). 23
- Figure 13.** Probability density curves of peak (left) and background (right) ozone mixing ratio during thunderstorm days (red lines). 24
- Figure 14.** Probability density curves of peak (left) and background (right) ozone mixing ratio during cold front days (red lines) and post front days (purple lines). 25
- Figure 15.** Boxplot of peak ozone (upper) and background ozone (lower) mixing ratio during events. 26
- Figure 16.** Overlapping percentages between all types of meteorological events. 27
- Figure 17.** Seasonal co-occurrence of high ozone events with meteorological events. 28
- Figure 18.** Contribution of background ozone (left) and mean background ozone (right) during event days. 29
- Figure 19.** Count of exceedance days with adjusted background ozone (left column) and local ozone (right column). 30
- Figure 20.** 3-day back trajectories of the Central America group (a) and clean-Gulf group (b) for May 2008. 31
- Figure 21.** HGB background ozone grouped by air mass origins identified by back trajectory for Apr-May from 2000 to 2015. 32

Figure 22. Time series of simulated daily HGB MDA8 ozone (fire-on and fire-off), observed HGB MDA8 ozone, and observed HGB background ozone in April 2011 (left) and May 2008 (right). 33

Figure 23. Time series of simulated ozone enhancement at HGB during April 2011 (left) and May 2008 (right). 33

Figure 24. HGB background ozone grouped by air mass origins identified by GEOS-Chem passive tracer simulation and burnt area for Apr-May from 2002 to 2015. 34

Figure 25. MOPITT CO total column observations for the fire-impact days (left), clean-Gulf days (middle), and the difference between fire-impact days and clean-Gulf days (right). The sampling period is for April and May from 2002 to 2015. 35

Figure 26. MODIS AOD observations from Terra satellite for the fire-impact days (left), clean-Gulf days (middle), and the difference between fire-impact days and clean-Gulf days (right). The sampling period is for April and May from 2002 to 2015. 36

List of Tables

Table 1. Performance metrics of the GEOS-Chem model. 17

1. Introduction

Exposure to ozone remains a significant public health issue in the United States (US). The Houston-Galveston-Brazoria (HGB) area exceeds the US National Ambient Air Quality Standard (NAAQS) for ozone (TCEQ, 2012). For the purpose of source attribution, surface O₃ over the HGB can be conceptually considered to be the sum of those produced locally added onto a 'regional background'. By definition, this background ozone originates from both pollutions emitted outside of Texas and natural sources, thereby considered not directly controllable at the local and state levels. Berlin et al. (2013) found that background ozone contributes more than 50% to the HGB MDA8 ozone and explains 63-83% of the MDA8 ozone variability during the ozone season. Given this substantial contribution, this report aims at identifying extreme events of high background ozone over the HGB area over a longer time period, plus characterizing common features and drivers of these events, and understanding their effects on ozone exceedance.

Episodic emissions such as fires are important drivers of short-term enhancement in background ozone (Morris et al., 2006). Significant progress has been made in the past to improve emission estimates from wildfires and quantify the impacts of these emissions on Texas air quality, with a focus on fires from the continental U.S. (Kemball-Cook et al., 2014; McDonald-Buller et al., 2015). Internationally, Mexico and Central America is a large fire region of unique importance to Texas air quality and its background ozone. The Central America fire season peaks in spring (Apr-May), coincident with the start of the ozone season in Texas. Satellite and in situ measurements have documented several cases of long-range transport of fire smokes and gaseous emissions from the Yucatan Peninsula and Central America across the Gulf of Mexico into Texas and other parts of the southern U.S. (Wang et al., 2006; Alvarez, 2009). The transport of Central American fire emissions into Texas is largely steered by the Bermuda High (Wang et al., 2009), the same large-scale circulation pattern controlling the

maritime background ozone into the HGB area. The implication of this linkage on HGB background ozone has not been investigated in prior analyses.

Out-of-state emissions and meteorology are two independent factors controlling background ozone, whose effects can be quantified separately. This report investigates and quantitatively estimates the role of meteorology on surface ozone and background ozone in the HGB region during the long-term period of 2000-2015, focusing on Apr-Oct of each year, the peak months of background ozone in HGB. For emission, we focus on the impact of Central American biomass burning on HGB background ozone for April and May from 2000-2015.

2. Methods

2.1 Study Area

The red box in Figure 1 shows the research area including the region of Houston, Galveston, and Brazoria (HGB), delineated by latitude from 28.5°N to 30.5°N, and by longitude from -94.5°W to -96.0°W.

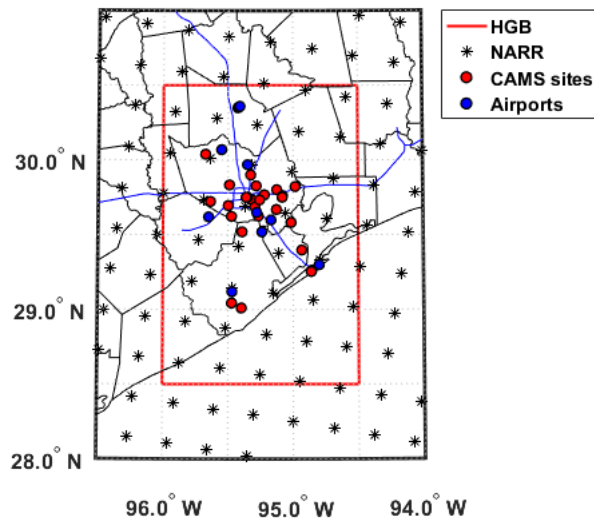


Figure 1. Research area: the HGB region (red box), NARR reanalysis data points (*), CAMS sites (red dots), and airports (blue dots) with thunderstorm information.

2.2 Ozone Data and Meteorological Data

MDA8 ozone concentrations in the state of Texas have been routinely monitored at continuous ambient monitoring stations (CAMs) (red dots in Figure 1) maintained by the Texas Commission on Environmental Quality (TCEQ) and other entities. In our study, observational records of MDA8 ozone during the ozone season (April 1 - October 31) from 2000 to 2015 over HGB region were obtained from the TCEQ website (https://www.tceq.texas.gov/cgi-bin/compliance/monops/8hr_monthly.pl). The background ozone and peak ozone mixing ratios over the HGB region during the ozone season (April 1- October 31) from 2000 to 2015 were provided by Mr. Mark Estes at TCEQ (Estes et al., 2014; Berlin et al., 2013). All the ozone data in the report refer to MDA8 ozone unless stated otherwise.

The National Centers for Environmental Prediction (NCEP) and North American Regional Reanalysis (NARR) products of wind speed, temperature and precipitation were used. The products have a spatial resolution of 32 km × 32 km horizontally (data points shown as “*” in Figure 1) with 45 vertical layers, and temporal resolution of every 3 hours from 1979 to present, based on observations used in NCEP/NCAR Global Reanalysis project (<http://rda.ucar.edu/datasets/ds608.0/>). Wind speed, temperature, and precipitation over the HGB area were extracted from the NARR data set. Thunderstorm data were extracted from historical weather records of 9 airports (blue dots in Figure 1) in the HGB area from Weather Underground (<https://www.wunderground.com>).

Cold front data was obtained from the Weather Prediction Center (WPC) Surface Analysis, which is part of the National Weather Service (NWS) Unified Surface Analysis and a collaborative effort with the Ocean Prediction Center (OPC) and the National Hurricane Center (NHC). It is a manual analysis of surface front locations and pressures over North America and adjacent oceans at 3-hour intervals from 2003 to present. They utilize a variety of weather data in addition to observations of surface weather conditions, such as upper air observations,

global satellite imagery, Doppler radar, and model mass fields to ensure that the product is meteorologically consistent and of the highest quality. Figure 2 shows a sample weather map of the WPC surface analysis valid for 04/04/2014 at 12 UTC when a cold front crossed the HGB.

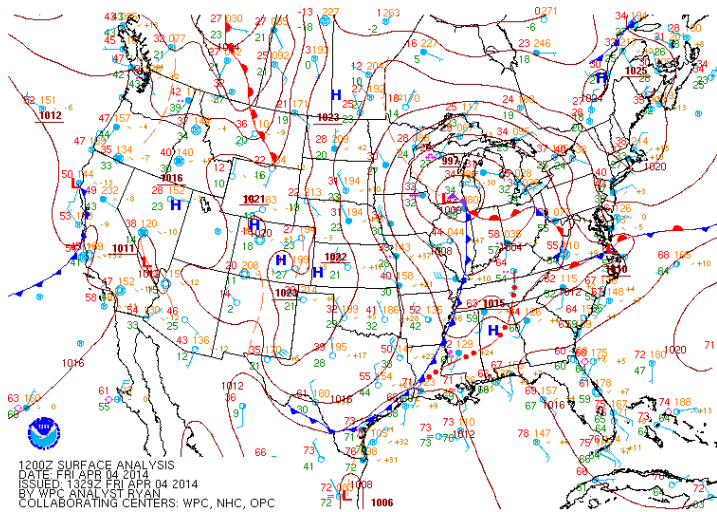


Figure 2. Weather map sample of the WPC surface analysis valid for 04/04/2014 at 12 UTC.

2.3 Satellite Data

The Measurements of Pollution in the Troposphere (MOPITT) is an instrument on-board the NASA Terra polar-orbiting satellite, which measures tropospheric carbon monoxide (CO) globally and has been operated since 2000. MOPITT measures CO in two channels: thermal-infrared (TIR) band (4.7 μm) and near-infrared (NIR) band (2.3 μm). The NIR measurements are sensitive to the total column while TIR radiances are sensitive to CO in middle and upper troposphere. In this study, MOPITT Level 3 Version 7(V7) TIR-NIR daily mean gridded ($1^\circ \times 1^\circ$) CO products were used, which exploits both NIR and TIR channels. The TIR-NIR product has high sensitivity to CO in the troposphere compared to previous TIR-only product (Worden et al., 2010). Only daytime MOPITT observations were used because Central American fires mostly occur in the daytime and there is no sensitivity near the surface for NIR channel during nighttime.

The MODerate-resolution Imaging Spectroradiometer (MODIS) onboard both the Terra and Aqua satellite provide aerosol products including aerosol optical depth (AOD) globally. We used

AOD products from Terra MODIS Level 2 Collection 6 with a spatial resolution of 10 km x 10 km at 550 nm wavelength.

2.4 High ozone events and meteorological Events

Three types of high ozone events were identified for HGB: ozone exceedance days, top 15% peak ozone days, and top 15% background ozone days. Ozone exceedance days are defined as the days when at least two surface monitors in HGB exceeded 70 ppbv. The definition of exceedance based on two monitors reduces the influence of local emissions specific to any single site on the analysis. Top 15% peak ozone days are defined as the 15% highest peak ozone days in each single month, corresponding to a total of 4 days per month. Use of the top 15% standard is to include those relatively high ozone days in years and months with fewer exceedances, considering the declining trend of exceedance days during the study period. The top 15% background ozone days are defined as the 15% highest background ozone days in each single month, corresponding to a total of 4 days per month.

Five types of meteorological events were identified for HGB: heat wave, stagnation, thunderstorm, cold front, and post front. A heat wave day is defined when the daily maximum temperature at a given location exceeds the “climatological” daily maximum temperature by at least 5 K for more than two consecutive days. A stagnation episode is defined when the 10 m wind speed, 500 hPa wind speed, and precipitation at a given location over a three-hour period (the temporal resolution of the NARR dataset) are all less than their climatological values for the reference by at least 20%. If a stagnation episode appeared at any time point in a day, we call it a stagnation day. Definitions of heat wave and stagnation are adopted from the study of Hou et al. (2016) which is a global analysis using the coarse-resolution (2.5° latitude by 2.5° longitude) NCEP reanalysis data which cannot resolve the HGB region. They used 1961-1990 as the reference period to calculate the ‘climatological’ conditions for stagnation and heat wave. Since the NARR data is available 1979 - present, we chose a 20-year period 1979 - 1998 as the

climatological reference. We first calculated the extreme events by grids. For a certain day, if more than half of the NARR grids in the HGB land region show heat wave or stagnation, we call it an HGB heat wave day or stagnation day.

A thunderstorm day is defined as when more than one airports in HGB reported thunderstorms. This definition is similar to that of ozone exceedance based on the CAMS network. A cold front day is defined as the day when a cold front line passed the HGB area at one or more 3-hour frames. Since surface ozone would change after a cold front passes, post front should be treat as a separate event. A post front day is defined as the day on which no cold front line passed the HGB area but the previous day was a cold front day.

2.5 Background ozone contribution

To quantify the effect of background ozone on total ozone over the HGB area, we define the percentage contribution of background ozone to peak ozone as follows:

$$\text{Contribution} = (\text{Background ozone mixing ratio}) / (\text{Peak ozone mixing ratio}) * 100\% \quad (1)$$

The time periods for the background ozone and peak ozone are the same, both as daily values. To quantify the contribution of background ozone to site-level exceedance, we assume background ozone at each of the 28 CAMS sites is the same as the daily background ozone over the whole HGB area. Local ozone for each site thus can be defined as follows:

$$\text{Local ozone} = \text{site-level ozone} - \text{background ozone} \quad (2)$$

With the local ozone and background ozone component identified at each CAMS site and assuming they are independent to each other, we can calculate the hypothetical level of ozone mixing ratio (referred to as adjusted ozone) at each CAMS site resulting from a given perturbation to background ozone (r1) and/or local ozone (r2), following equation (3):

$$\text{Adjusted ozone} = r1 * \text{Background ozone} + r2 * \text{Local ozone} \quad (3)$$

In this study we set the value of r1 and r2 to range from 100% (no perturbation) to 70% (i.e. 30% reduction) at an interval of 10%. Adjusted exceedance days are calculated by the same

definition of ozone exceedance days described above using the adjusted ozone mixing ratios at each CAMS site.

2.6 Back Trajectory

In order to identify the days which were affected by pollutant transport from Central American fires (referred to as fire-impact days), we used the Hybrid Single Particle Lagrangian Integrated Trajectory Model (HYSPLIT) to calculate the back trajectories of air masses at the HGB for April and May from 2000 to 2015. Back trajectories are driven by NARR at a resolution of 32 km x 32 km and calculated every three hours with the destination height at 1 km above the surface. The fire-impact days are the days with equal to or greater than four trajectories passing through the two main fire regions: the Yucatan Peninsula and Central Mexico as shown by box 1 and box 2 in Figure 3 respectively. As a contrast to the fire-impact days, clean-Gulf days were also selected, which are defined as the days with all the background trajectories originating in the Gulf of Mexico and without passing through the two fire domains.

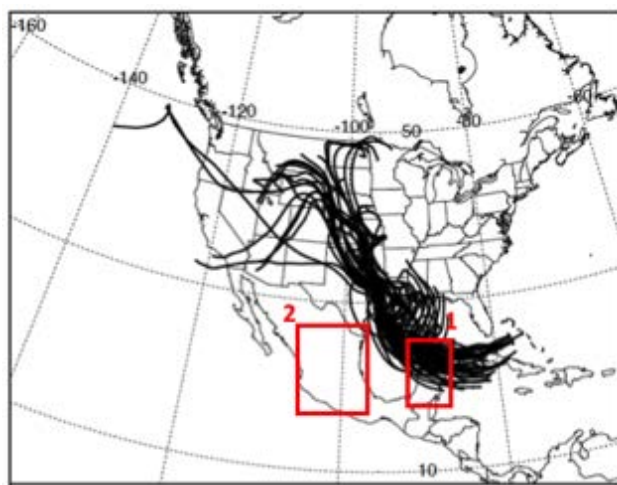


Figure 3. Two boxes are defined over the main fire emission sources in Central America.

Box 1 (17.23°N-21.65°N; 85.45°W-91.79°W) represents the sources in the Yucatan Peninsula.

Box 2 (16.35°N-25.97°N; 97.59°W-105.72°W) represents the sources in Central Mexico.

2.7 GEOS-Chem model

We conducted GEOS-Chem passive tracer simulations (v11-01) in the global and nested North America domain. Those simulations were driven by the reanalysis meteorology from Modern Era Retrospective-analysis for Research and Applications, Version 2 (MERRA-2). The MERRA-2 data provides consistent 30-year reanalysis, suitable for the 2000-2015 long-term simulations required by the project. The global simulation was used to provide boundary conditions, and the nested-grid simulation over North America with a horizontal resolution of 0.5° latitude x 0.625° longitude was used for analysis. The passive tracer simulation in GEOS-Chem was designed with six synthetic passive tracers. Each tracer has a fixed lifetime of 30 days, which resembles CO lifetime in the warm season, and those tracers were emitted at a constant rate from the following six source regions of importance to HGB: Houston, Texas (excluding Houston), US (excluding TX), Gulf of Mexico (referred to as the Gulf tracer), Mexico, and the Rest of Central America (RCA). Figure 4 shows the masks of each source region. The major source regions affecting HGB on daily basis were determined with these passive tracers.

The nested-grid GEOS-Chem model with tropospheric chemistry mechanism was used to conduct sensitivity simulations of ozone chemistry for selected months to quantify ozone enhancements at HGB due to Central American fires. The model used the Fire INventory from NCAR version 1.0 (FINNv1) which provides emissions of tracer gases and particles from open biomass burning in daily scale at a 1-km spatial resolution (Wiedinmyer et al., 2011). Long-range transported effects of Central American fires on HGB surface ozone were quantified through the difference in model results with and without fire emissions in Central America.

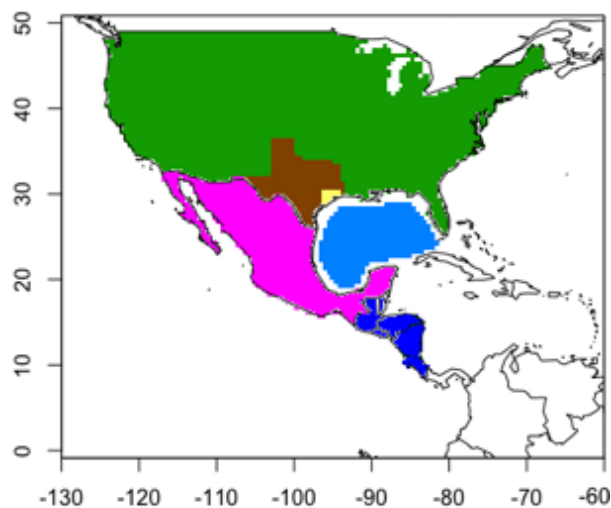


Figure 4. Source regions of the six passive tracers in GEOS-Chem: US (excluding Texas; green), Texas (excluding Houston; brown), Houston (yellow), Mexico (pink), Gulf of Mexico (light blue), and the rest of Central America (RCA; dark blue). The mask file is at a resolution of $0.5^\circ \times 0.5^\circ$.

2.8 GEOS-Chem-based selection of fire-impact days

We used two criteria to select the fire-impact days based on the results from GEOS-Chem passive tracer simulations in conjunction with burned area statistics estimated from FINN: (1) Simulated Mexico tracer at HGB exceeds 85-percentile of all days combined; and (2) Burn area over Central America exceeds 70-percentile of all days combined. Since the GEOS-Chem-based fire-impact days were selected on the basis of both transport (criteria 1) and source emissions (criteria 2), they are expected to be more accurate than those derived from back trajectories (2.6) which account for transport only. However, the two methods are independent and can be used to corroborate with each other. GEOS-Chem-based clean-Gulf days were also defined by both the transport and emissions criteria: (1) simulated Gulf tracer at HGB exceeds the 85-percentile of all days combined; and (2) Burn area over Central America lower than 70-percentile. The domain of burned area statistics retrieved from FINN is from 83.33 to 110°W by longitude, and from 10 to 26°N by latitude.

3. Quality Assurance/Quality Control Procedures

3.1 Quality of secondary data

The CAMSs data of MDA8 ozone over the HGB region were downloaded in ASCII format from the EPA website (<https://www3.epa.gov/airquality/airdata/>). Even though there are some missing data, the overall data coverage is good at 99%. Data were downloaded as daily mean and aggregated onto monthly mean. Before the monthly aggregation, daily data completeness was checked and outliers were examined and discarded.

3.2 Quality of GEOS-Chem modeling

The GEOS-Chem global chemical transport model has a standard benchmarking procedure for each major code release, using observations compiled from surface monitoring network, aircraft campaigns, and satellite retrievals around the globe. Building from these efforts, we performed in-depth evaluation of the model's performance in simulating surface ozone and its different components over the HGB region, using the performance metrics listed in Table 1. The GEOS-Chem model simulation results were thoroughly evaluated also using the benchmark observations in the continental US. Interactive Data Language (IDL) programs were used to visualize and extract the corresponding model outputs for the comparisons with the observational data. We have maintained documentation files for each model run that identifies model code versions, dates, analyst, and input and output files. Each input/output file used were reviewed for quality assurance purposes using various visualization methods, including software animations and graphing, as well by quantitative filtering using selected filter criteria to identify anomalous data.

Table 1. Performance metrics of the GEOS-Chem model.

Mean Bias (MB)	$MB = 1/N \sum_{i=1}^N (M_i - O_i)$
Normalized Mean Bias (NMB)	$NMB = \frac{\sum_{i=1}^N (M_i - O_i)}{\sum_{i=1}^N O_i} \times 100\%$
Correlation Coefficient (Corr. R)	$Corr.R = \frac{\sum_{i=1}^N (M_i - \bar{M})(O_i - \bar{O})}{\sqrt{\sum_{i=1}^N (M_i - \bar{M})^2} \sqrt{\sum_{i=1}^N (O_i - \bar{O})^2}}$
Root Mean Square Error (RMSE)	$RMSE = \sqrt{1/N \sum_{i=1}^N (M_i - O_i)^2}$

Note: M is the model output, O is the observation, N is the number of samples, and

$$\bar{M} = 1/N \sum_{i=1}^N M_i, \bar{O} = 1/N \sum_{i=1}^N O_i.$$

4. Results

4.1 Ozone Time Series

Figure 5 shows the ozone season (April to October) mean peak ozone and background ozone time series over the HGB region, with both showing a declining trend in 2000-2015. Peak ozone decreases faster than background ozone with a more significant trend, indicating the key role of in-state emissions control in reducing ozone at HGB. For month-to-month variability, both peak ozone and background ozone show a minimum in July, attributable to the strong maritime inflow driven by the Bermuda High circulation (Wang et al., 2016).

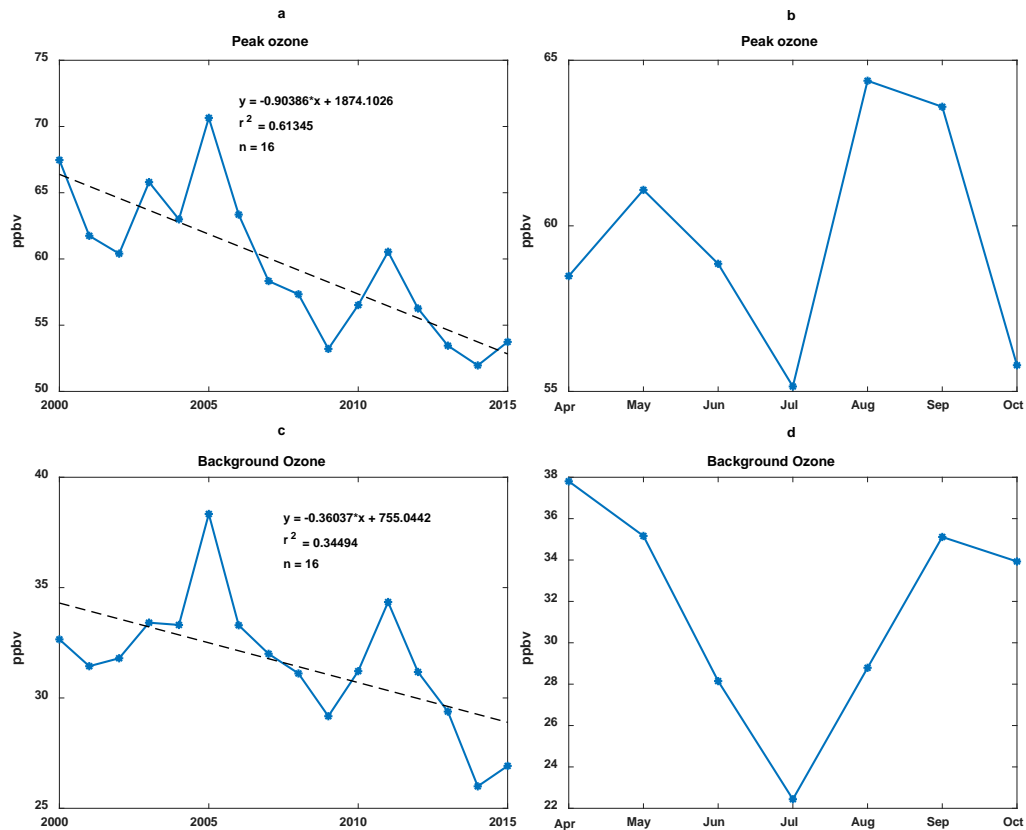


Figure 5. Year (left column) and monthly (right column) time series of average peak MDA8 (lower row) and background (upper row) ozone mixing ratio.

Figure 6 shows mean ozone mixing ratio during each type of the high ozone events defined in 2.4. Ozone decreases faster during those high-ozone events than the all-day mean as shown in Figure 5. Both top 15% peak ozone and top 15% background ozone show a large declining trend than the exceedance-day peak ozone. This is because the top 15% criteria contain relatively more exceedance days in the earlier years than the later years as the number of exceedance days declines with time.

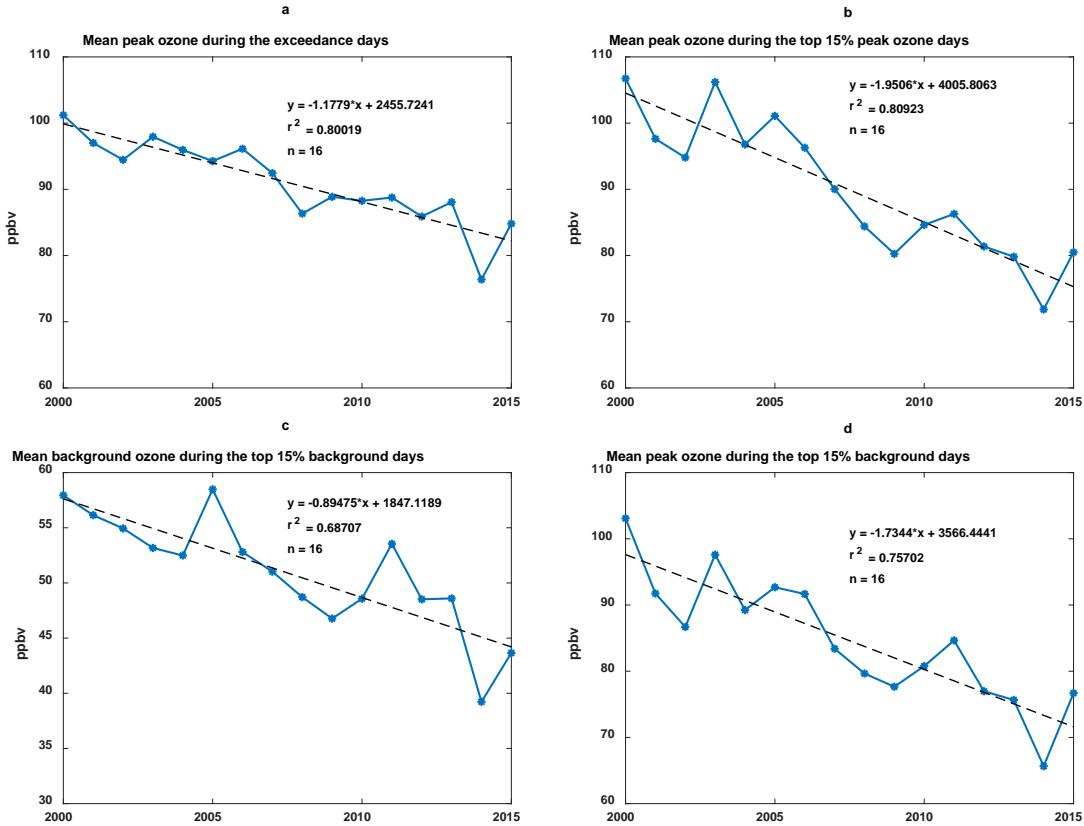


Figure 6. Year time series of mean peak ozone during exceedance days (top left), mean peak ozone during the top 15% peak ozone days (top right), mean background ozone during the top 15% background ozone days (bottom left), and mean peak ozone during the top 15% background ozone days (bottom right).

4.2 Events time series

Figure 7 shows the time series of the yearly and monthly count of ozone exceedance days. The mean count was 38.44 days per year with a significant decreasing trend. The first peak appeared on 2005 with 64 days per year. The minimum, 8 days per year, appeared in 2014. The second peak appeared in 2010 and 2011, which were 34 days per year. The monthly count shows a double-peak distribution. The maximum count appeared on August which was a total of 132 days over 2000-2015, with the minimum count of 53 days in July.

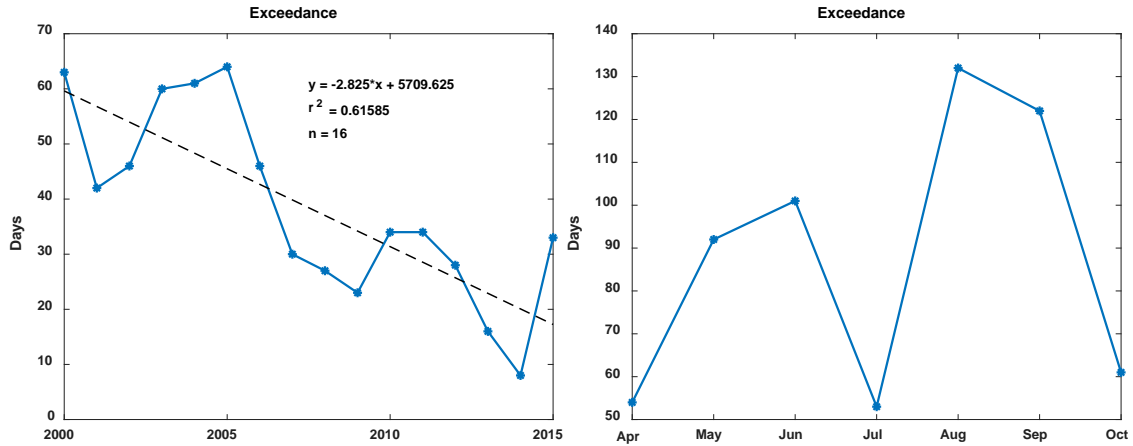


Figure 7. Year (left) and monthly (right) time series of exceedance days.

Since the top 15% ozone days are always 4 days per month by definition, no plots were presented for the count of top 15% peak ozone days and top 15% background days.

Figure 8 shows the time series of annual and monthly count of heat wave days. Heat waves have large interannual variability, with a peak in 2011 (67 days per year) and no occurrences in a number of years (e.g. 2003, 2007, 2008, 2014, and 2015). For monthly count, the maximum appeared in April and June which totaled 30 days over 2000-2015, with the minimum of 8 days in July. Given its extremely uneven distribution, the effects of heat wave on HGB ozone distributions were not included in the rest of this report.

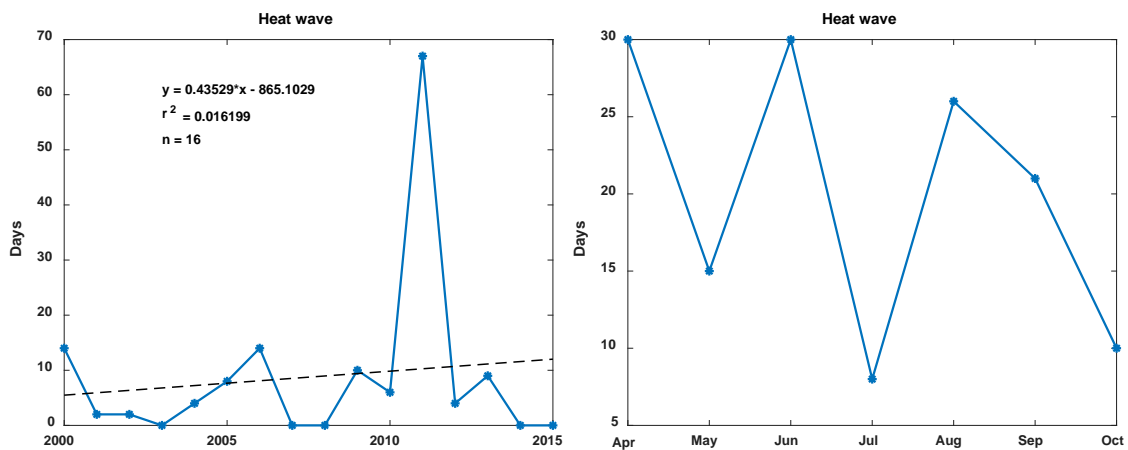


Figure 8. Year (left) and monthly (right) time series of heat wave days.

Figure 9 shows the time series of year and monthly count of stagnation days. For annual

count, it varied between 13 (2013) and 41 days (2007) with a mean of 28.38 days per year. For monthly count, the maximum appeared in October with a total of 94 days and the minimum in August of 44 days. There was a second peak in June with a total of 83 days.

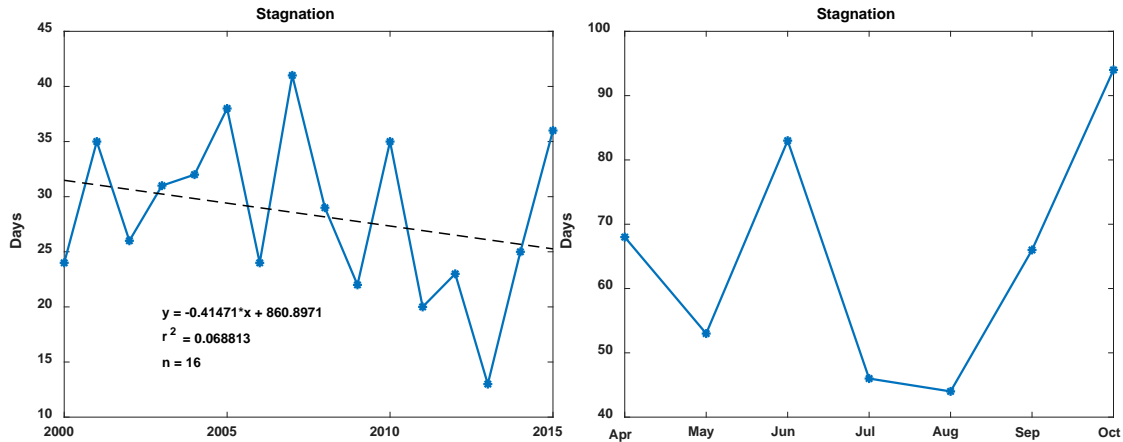


Figure 9. Year (left) and monthly (right) time series of stagnation days.

Figure 10 shows the annual and monthly time series of thunderstorm days. The average thunderstorm day occurrence was 76 days per year, making it the most frequent weather event in this study. The co-occurrence of thunderstorm trough and heat wave peak in 2011 may explain the exceedance peak in that year when a severe drought hit Texas. The monthly series showed a single peak in July.

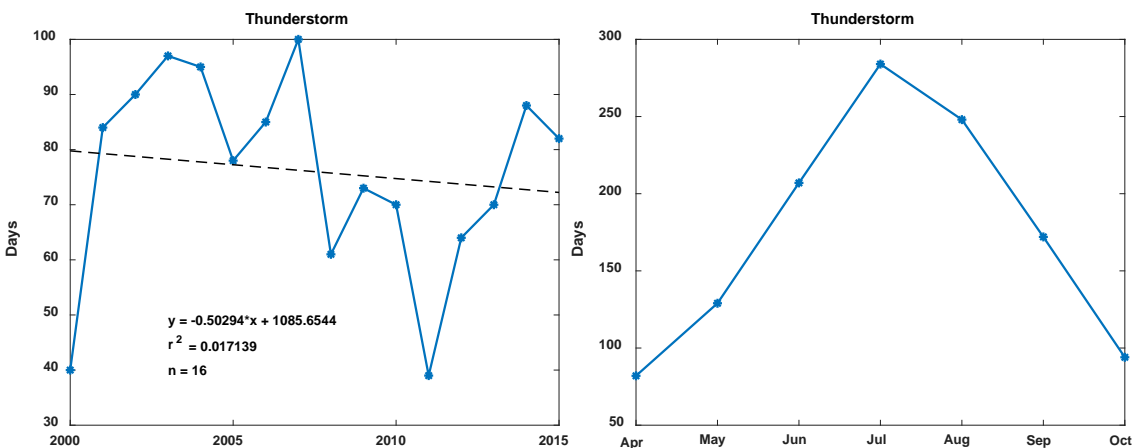


Figure 10. Year (left) and monthly (right) time series of thunderstorm days.

The cold front data starts from 2003. Figure 11 shows monthly and yearly time series of the count of cold front days at HGB. Totally there were 389 cold front days during April – October of 2003 – 2015. On average cold front occurred 29.92 days per year. There was no significant trend, given the large year-to-year variability ranging from 21 days in 2010 to 44 days in 2009. For monthly variation, the occurrence peaks appeared the in April and October, both reaching 90 days in the 13-year period, with the summertime (June – Aug) occurrence lower than 35 days during the 13-year period.

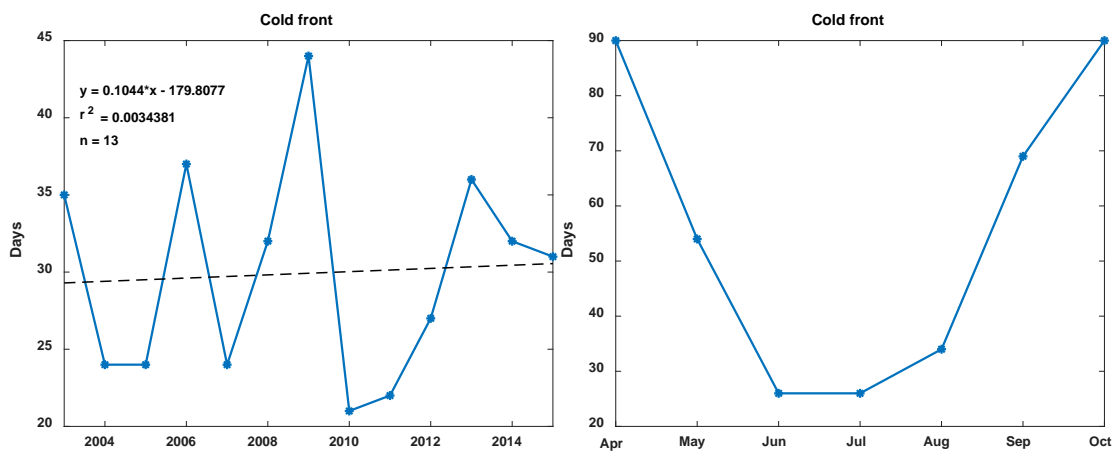


Figure 11. Year (left) and monthly (right) time series of cold front days.

4.3 Ozone distribution changes during events

Probability density curves of ozone distributions were plotted to examine the effects of meteorological events. For the convenience of comparison, peak ozone and background ozone distributions are plotted separately in Figure 12-14. The all-data population, exceedance-day population, and top 15%-day population are shown in each Figure as references to compare with the ozone distribution during different meteorological events. For peak ozone, the mode of all data, exceedance-day data, and top 15%-day data is 47, 88, and 84 ppbv respectively. For background ozone, the mode of all data, exceedance-day, and top 15%-day data is 18, 54, and 53 ppbv respectively.

Figure 12 shows the probability density curves of peak and background ozone mixing ratios during stagnation days. The mode of stagnation-day distribution is 81 and 50 ppbv for peak ozone and background ozone, respectively. Stagnation thus has a large increasing effect on both peak and background ozone as it shifts the mode of their respective distributions very close to those during the high ozone days.

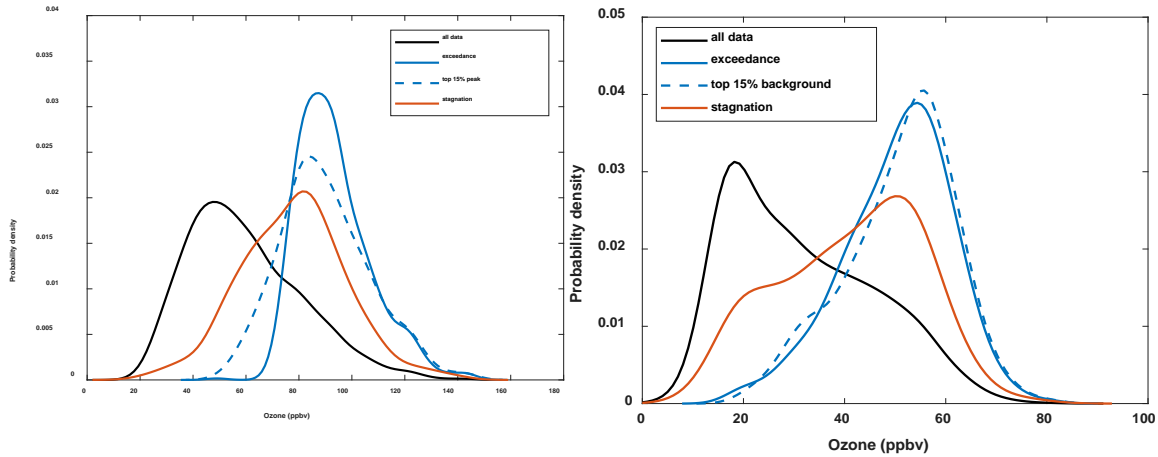


Figure 12. Probability density curves of peak (left) and background (right) ozone mixing ratio during stagnation days (red lines).

Figure 13 shows the probability density curves of peak and background ozone mixing ratios during thunderstorm days. The mode of thunderstorm-day distribution is 42 and 17 ppbv for peak ozone and background ozone, respectively. Thunderstorm has a decreasing effect on both peak and background ozone as it reduces the right tail of the ozone distribution as well as shifts the mode of their respective distributions slightly to the left of the all-data curve. Although lightning during thunderstorm may produce NO_x that produces ozone, precipitation and convection may offset that effect and play a dominant role in lowering surface ozone.

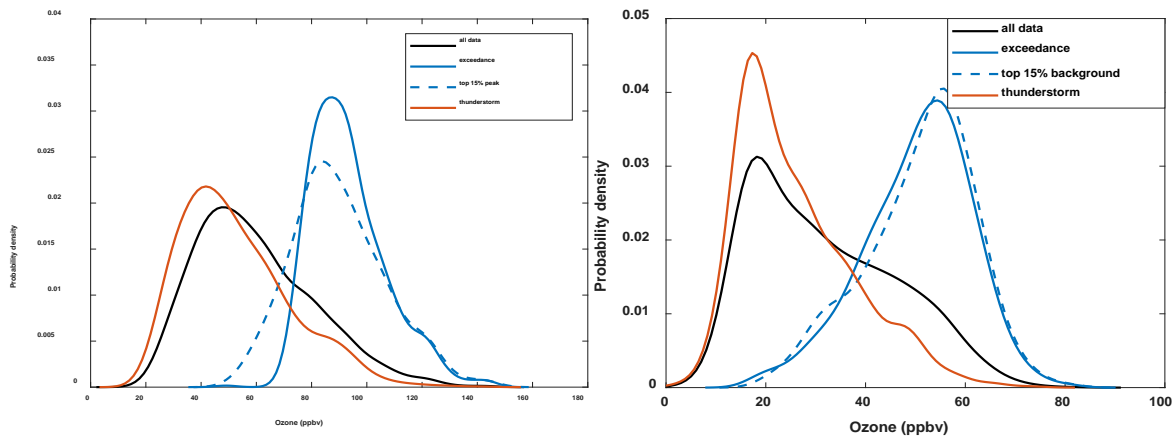


Figure 13. Probability density curves of peak (left) and background (right) ozone mixing ratio during thunderstorm days (red lines).

Figure 14 shows the probability density curves of peak and background ozone mixing ratios during cold front and post front days. The mode of cold front day distribution is 57 and 32 ppbv for peak ozone and background ozone, respectively. By comparison, the mode of post front day distribution is significantly higher, at 64 and 43 ppbv for peak and background ozone, respectively. A cold front may have confounding effects on HGB ozone by bringing in polluted air masses from the north and northeast and causing lower temperatures which likely lead to low ozone production rates. Based on the distribution changes, it seems the increasing effect outweighed the decreasing effect on daily ozone over the HGB area. The increasing effect of cold front on the HGB ozone was intensified during post front days. This may be because the low temperature in cold front day had recovered but northerly flow with ozone precursors had not stopped.

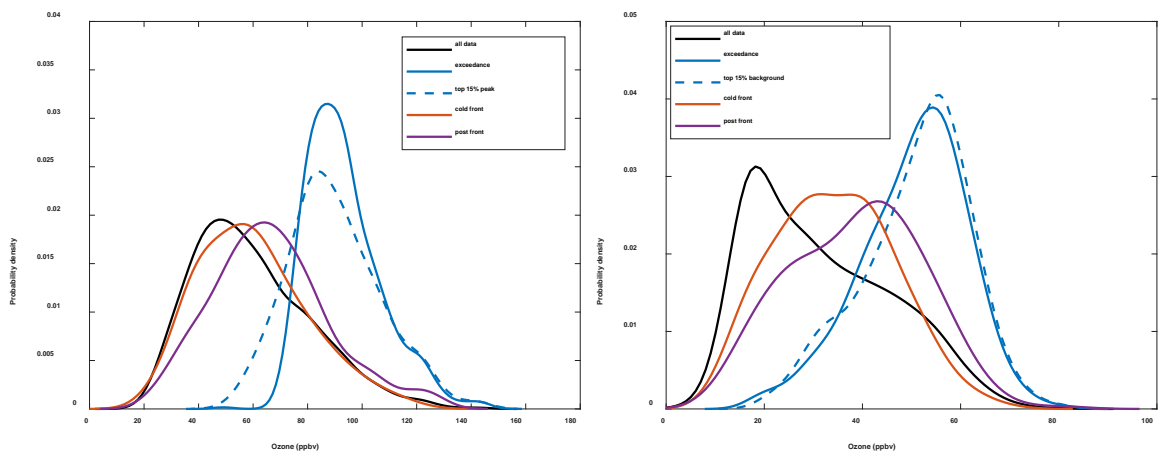


Figure 14. Probability density curves of peak (left) and background (right) ozone mixing ratio during cold front days (red lines) and post front days (purple lines).

As a summary, Figure 15 shows ozone mixing ratio distributions during all the event days and their respective non-event counterparts. The median differences in peak ozone between event and non-event days are 39, 36, 30, 26, -11, 3, and 11 ppbv for exceedance, top 15% peak ozone, top 15% background ozone, stagnation, thunderstorm, cold front, and post front days respectively. The corresponding differences for background ozone are 27, 23, 27, 16, -10, 6, and 12 ppbv, respectively.

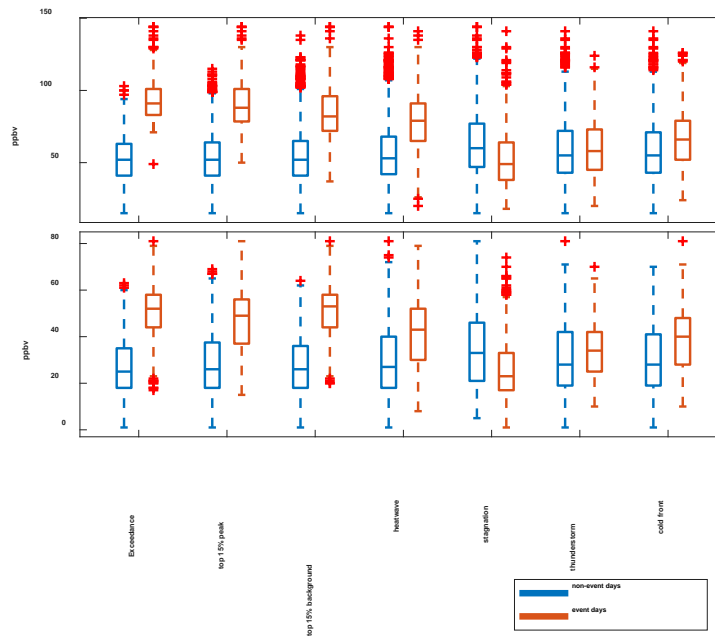


Figure 15. Boxplot of peak ozone (upper) and background ozone (lower) mixing ratio during events.

4.4 Co-occurrence of events

We first examine the extent to which the different meteorological events overlap with each other. Figure 16 shows the overlapping statistics between all types of meteorological events examined. Total overlapping percentages of heatwave, stagnation, thunderstorm, cold front, and post front days with other types of meteorological events are 30.33%, 58.27%, 34.03%, 61.95%, and 36.50%, respectively. Heatwave has the least overlapping rate with other events. Thunderstorm has the largest overlapping rate with other events because of its high frequency. For example, about 40% of cold front days are also identified as thunderstorm days, and 30% of stagnation days overlap with thunderstorm days. Given the sporadic nature of thunderstorm, our method of identifying thunderstorm, which is based on airport reports, may overestimate its effect for the HGB region as a whole. Excluding thunderstorm, the overlapping rate between the other meteorological events is all less than 20%.

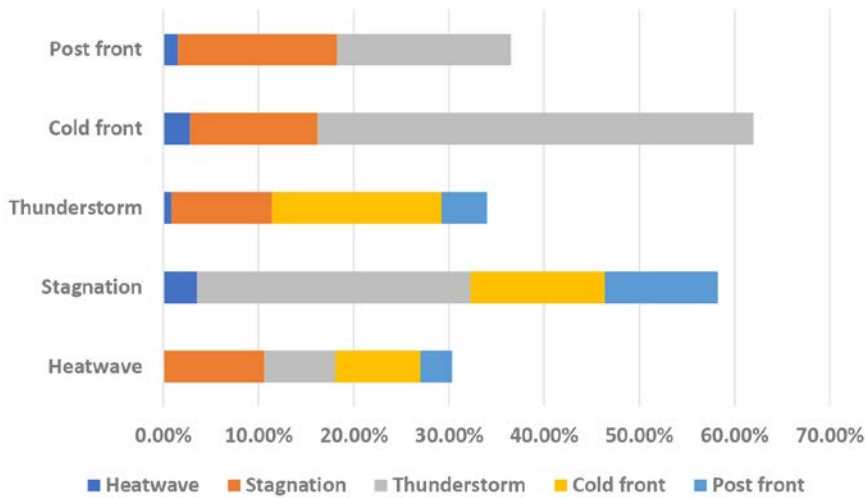


Figure 16. Overlapping percentages between all types of meteorological events.

Figure 17 shows the seasonal co-occurrence of high ozone events with meteorological events. The co-occurrence rate (%) is defined as the ratio of the number of days when a certain type of meteorological event coincides with a certain type of high ozone event divided by the total number of the high ozone event. Since the top 15% high ozone events (both background and peak ozone) are always 4 days per month as they are defined with respect to ozone data of every single month, the intra-seasonal variability of ozone mixing ratios are unlikely to affect the seasonal-mean co-occurrence rate for these two types of high ozone events. Such variability may affect the seasonal-mean co-occurrence rate for the exceedance events.

For stagnation, its co-occurrence rate with exceedance days is always higher than 30% in all the seasons. The co-occurrence rate with top 15% peak ozone and top 15% background ozone is less than that with exceedance but still much higher than other meteorological events except for thunderstorm during summer.

Thunderstorm has the largest seasonal variability in its co-occurrence rates with high ozone days. Although thunderstorm shows an overall decreasing effect on ozone mixing ratio, because of its high occurrence frequency during summer, it has higher co-occurrence rate with high ozone days than stagnation in summer. Sporadic nature of may be another reason why high

ozone events could happen during some thunderstorm days.

Both cold front and post front have 10-20% co-occurrence rates with high ozone events, despite that post front tend to be associated with higher ozone mixing ratio according to the above analyses. Their co-occurrence rates in spring are slightly higher than other seasons.

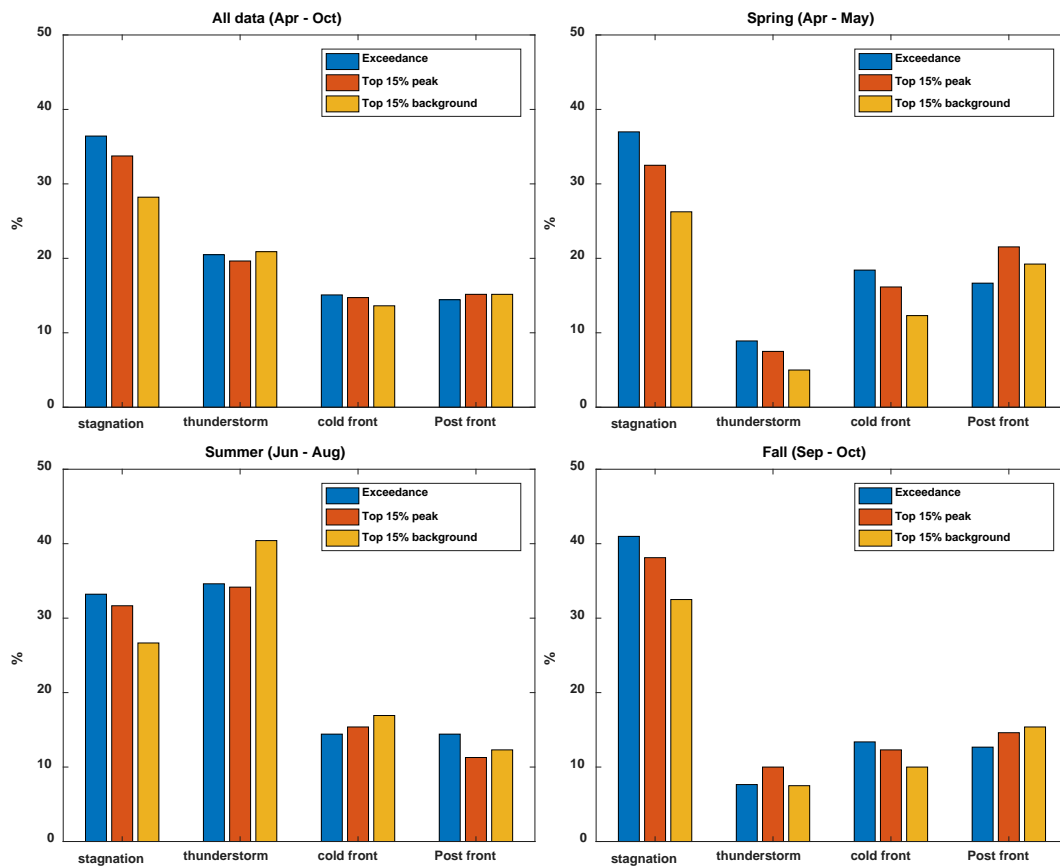


Figure 17. Seasonal co-occurrence of high ozone events with meteorological events.

4.5 Contribution of background ozone to peak ozone by event

Figure 18 shows the contribution (%) of background ozone to peak ozone as a function of different events and the mean background ozone mixing ratio during each type of events. The events are ranked by the median value of the background ozone contribution. The median contribution of background ozone to peak ozone is 53.66%, 60.56%, 58.33%, 55.91%, 54.82%,

53.85%, 50.00% for all data, post front, cold front, exceedance, stagnation, top 15% peak ozone, and thunderstorm respectively.

Post front days show the highest background contribution because of the large transport effects associated with them. Because of the transport effect, both cold front and post front days have higher background ozone contribution than exceedance days, although mean background ozone levels are lower than those during exceedance days.

Stagnation days show a similar background contribution with exceedance and top 15% peak ozone days. This is consistent with the similarity in ozone probability density curves between stagnation and the two high ozone events. Thunderstorm is the only event that shows a lower median contribution than the all-data population.

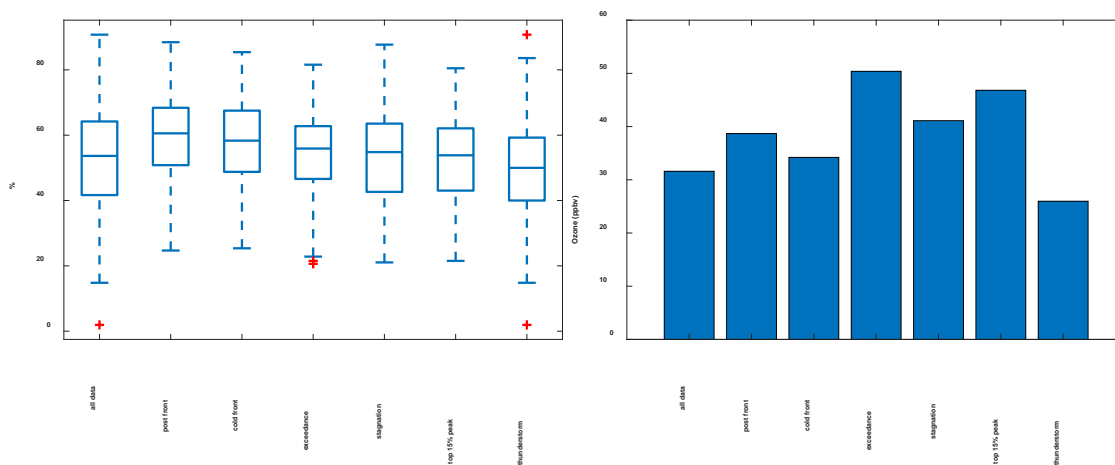


Figure 18. Contribution of background ozone (left) and mean background ozone (right) during event days.

Figure 19 shows the hypothetical counts of exceedance days based on adjusted ozone mixing ratios at the CAMS sites when background ozone and local ozone mixing ratios were reduced by 10-30% separately (c.f. equation 3 in Section 2.5). Note this hypothetical exercise was conducted to each day individually, thus it does not consider the possible effect of ozone left from the previous day that may be considered as “background”. The real number of HGB

ozone exceedance days during the 16 ozone seasons (April – October; 2000-2015) is 615 days. That number would be reduced to 486, 345, and 234 days if background ozone had been reduced by 10%, 20%, and 30% respectively with local ozone unchanged, and to 538, 458, and 366 days if local ozone had been reduced by 10%, 20%, and 30% respectively with background ozone unchanged. This means about 62% exceedance days would have been avoided at HGB if background ozone had been lower by 30%. By comparison, reducing local ozone by 30% would lead to only 40% reduction in the exceedance days. This comparison indicates the important role of background ozone on ozone exceedance at HGB. The monthly panels show similar results with background ozone reduction being more effective in reducing exceedance days at HGB, especially during the months of more exceedance days (i.e. May, Sep).

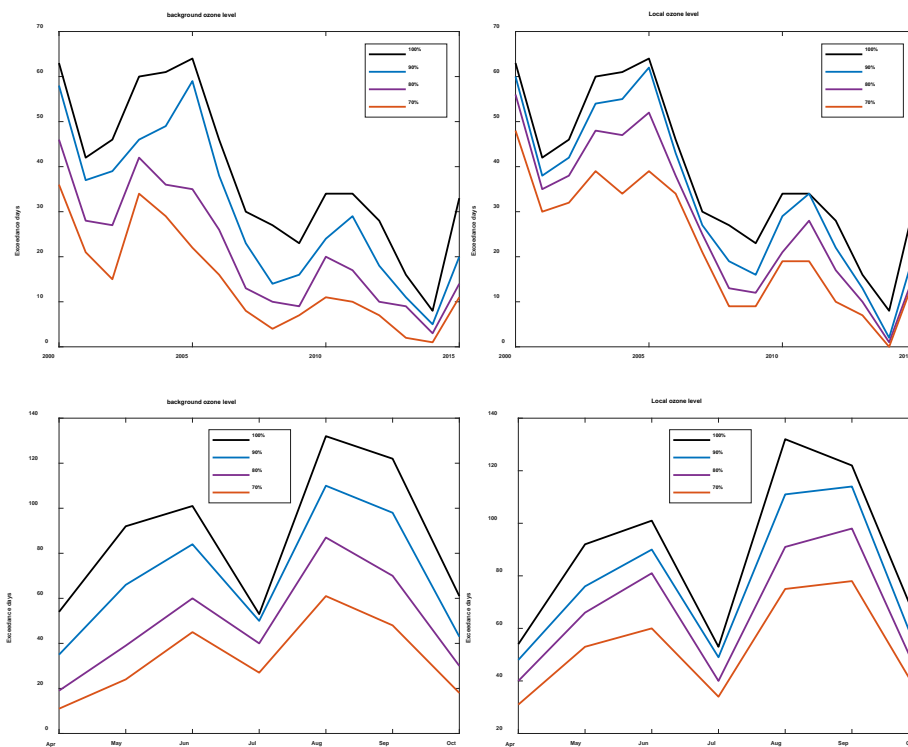


Figure 19. Count of exceedance days with adjusted background ozone (left column) and local ozone (right column).

4.6 Back trajectory analysis

As an example, Figure 20 shows the HYSPLIT 3-day back trajectories of the Central America group (a) and clean-Gulf group (b) for May 208. Trajectories in the Central America group mainly pass through the two fire source domains (i.e. box 1 and 2 in Figure 3) with only a few ones from the north. For the clean-Gulf group, almost all the trajectories are originated in the Gulf of Mexico and do not pass through source regions in land.

Figure 21 shows the mean HGB background ozone for April and May from 2000 to 2015 categorized by air mass origin. The air mass origin is determined by the HYSPLIT 3-day back trajectory. The all-data category includes all the background ozone observations from 2000 to 2015 April and May, which has the highest level of background ozone mixing ratio because it includes air masses from the north with higher background. Since the trajectories in the clean-Gulf group do not pass through polluted regions over land, the clean-Gulf group has the lowest background ozone mixing ratio and can be used as a reference to quantify the impact of Central American fires. Compared to the clean-Gulf group, the Central America group has mean background ozone enhancement of 5.67 ± 1.00 ppbv.

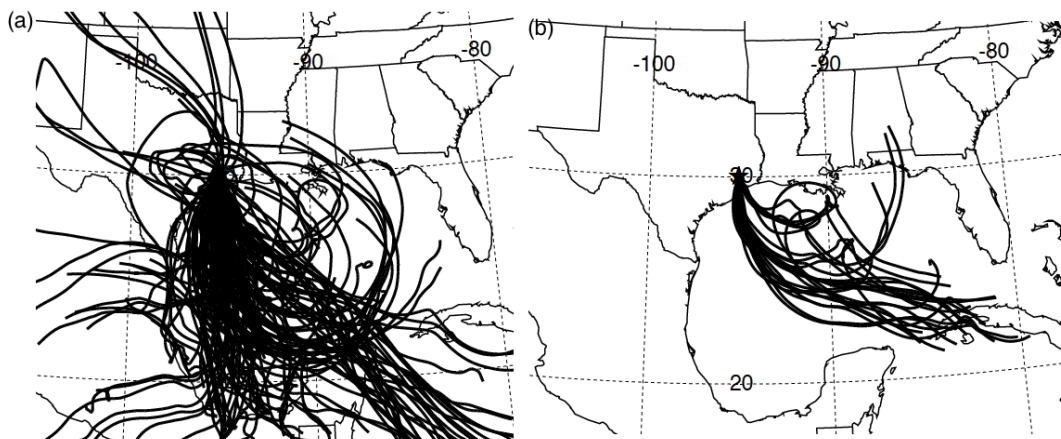


Figure 20. 3-day back trajectories of the Central America group (a) and clean-Gulf group (b) for May 2008.

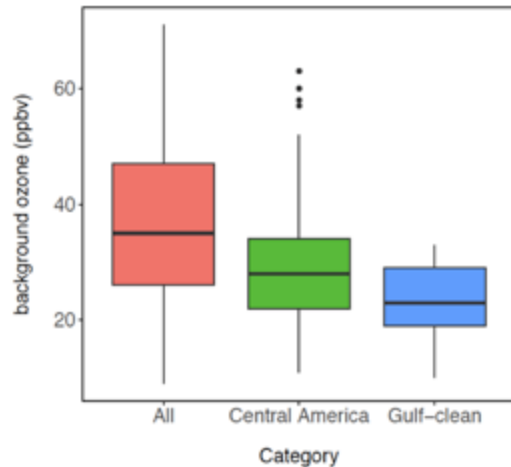


Figure 21. HGB background ozone grouped by air mass origins identified by back trajectory for Apr-May from 2000 to 2015.

4.7 GEOS-Chem simulation of fire cases

Two case months (April 2011 and May 2008) are selected to conduct the full chemistry GEOS-Chem simulation in order to quantify the fire impacts on HGB ozone. These two months were selected because they were identified as strong fire months by Saide et al (2015) and Saide et al (2016). Indeed, the burned areas of these two months exceeded 70-percentile of the burned areas for all April and May during 2002-2015, implying a potentially large impact of fires on the HGB ozone air quality. Figure 22 illustrates daily mean time series of observed (black line), simulated fire-on (blue line) and simulated fire-off (red line) O_3 over the HGB region. The observed background ozone (blue line) is also shown. Overall, the model captures the temporal patterns of observed daily mean ozone but it has a positive mean bias around 6.98 ppbv for April 2011 and 15.6 ppbv for May 2008, which is a common problem of current air quality models in simulating surface ozone along the Gulf Coast in absence of advanced halogen chemistry. The bias is high in some days when maritime flow prevails over the HGB region, which are identified by back trajectory, confirming the previous findings that the global models overestimate ozone in the marine boundary layer (MBL).

Figure 23 shows the time series of simulated ozone enhancement at HGB during April 2011 and May 2008. Ozone enhancement is defined as ozone simulated in standard model simulation minus ozone simulated by turning off Central American fire emissions (i.e. the difference between blue line and red line in Figure 22). The model indicates three episodes during April 11 and five episodes during May 2008, with the mean ozone enhancement of 5.59 ± 1.33 ppbv and 10.66 ± 3.86 ppbv respectively at HGB.

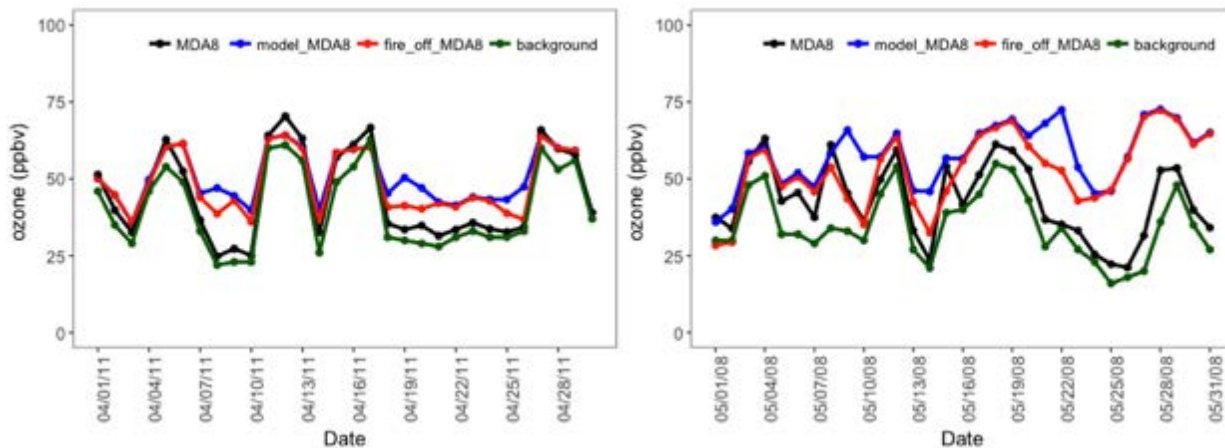


Figure 22. Time series of simulated daily HGB MDA8 ozone (fire-on and fire-off), observed HGB MDA8 ozone, and observed HGB background ozone in April 2011 (left) and May 2008 (right).

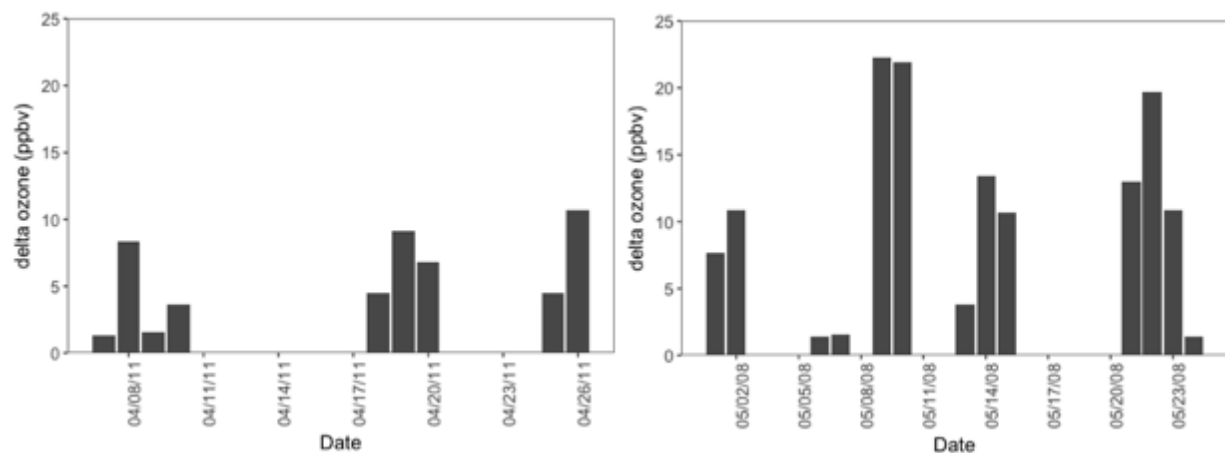


Figure 23. Time series of simulated ozone enhancement at HGB during April 2011 (left) and May 2008 (right).

4.8 Passive tracer simulation

Since the full chemistry sensitivity simulations are time consuming and computational expensive, passive tracer simulation provides an alternative way to sample the fire-impact days and clean-Gulf days. There are a total of 60 fire-impact days and 60 clean-Gulf days identified during the period of 2002-2015 (April and May of each year), using the method described in Section 2.8. Those days started 2002 instead of 2000 because burned area data were not available for 2000-2001, the GEOS-Chem-based fire-impact days cover the period of 2002-2015 (April and May of each year). Figure 24 shows the mean HGB background ozone for April and May from 2002 to 2015 categorized by the GEOS-Chem-based fire-impact and clean-Gulf days. Compared to the clean-Gulf days, the fire-impact days have a mean background ozone enhancement of 8.8 ± 1.6 ppbv. This enhancement is qualitatively consistent with the case study simulations but higher than that quantified by the back trajectory method (c.f. 4.6) because the GEOS-Chem-based passive tracer method considers the impact of burned area.

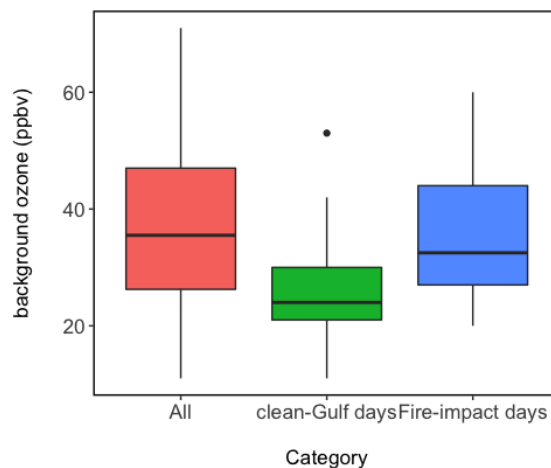


Figure 24. HGB background ozone grouped by air mass origins identified by GEOS-Chem passive tracer simulation and burnt area for Apr-May from 2002 to 2015.

4.9 Satellite observations

As a test of the validity of the GEOS-Chem passive tracer method, we used the GEOS-Chem-based fire-impact days and clean-Gulf days to sample the satellite data of CO and AOD during April-May 2002-2015 to verify if pollutant enhancements were detected by those satellite products during the fire-impact days as compared to the clean-Gulf days. Figure 25 shows the mean MOPITT CO observations of all the fire-impact days, clean-Gulf days and the difference between the two. CO is a major pollutant emitted in large quantity from biomass burning and has a longer lifetime (around 1-2 months) compared to other fire-emitted trace gases, so it is widely used to track the transport of fire plumes. During the fire-impact days, MOPITT shows CO enhancements originated in Mexico coastal cities and Guatemala reaching to Texas coastal cities (e.g. Corpus Christi and HGB), indicating the transportation of Central American fire plumes to the US. By comparison, during the clean-Gulf days, MOPITT sees much smaller CO signals over the fire source regions and CO tends to aggregate along the Mexican coast instead of spreading out. The total column enhancement of CO over the HGB region is around 2.03×10^{17} molec/cm², or 9.2% higher, compared to the clean-Gulf days.

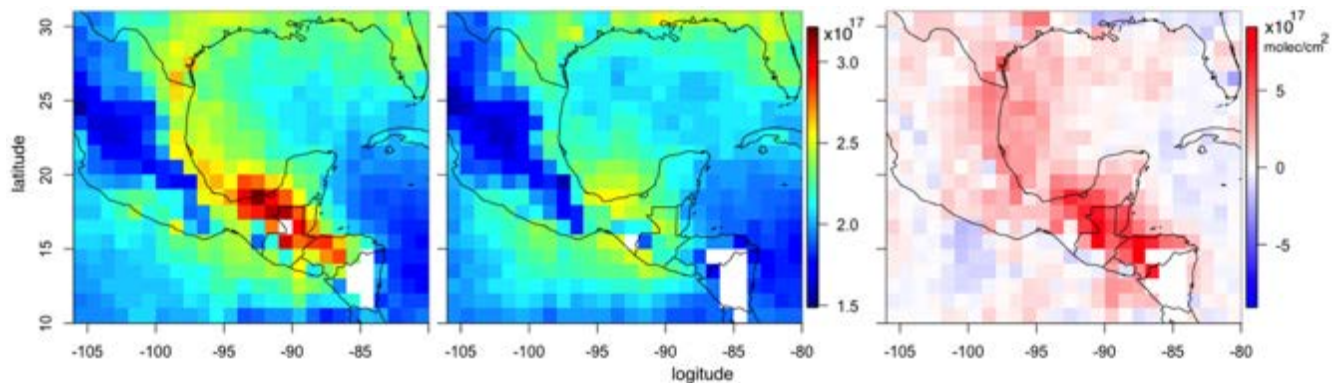


Figure 25. MOPITT CO total column observations for the fire-impact days (left), clean-Gulf days (middle), and the difference between fire-impact days and clean-Gulf days (right). The sampling period is for April and May from 2002 to 2015.

Figure 26 makes the similar comparison but for AOD from MODIS. Strong evidence of the Central American fire plumes transporting to southern US is also found in the AOD observations during the identified fire-impact days. The enhancement of AOD over the HGB region is around 0.04, or 19% higher, compared to the clean-Gulf days. To conclude, both MOPITT and MODIS detect significant enhancements of CO and AOD, respectively, along the transport route from Central America fires to HGB during the fire-impact days. This observational evidence supports the validity of the fire-impact days which were derived from the GEOS-Chem passive tracer described in Section 2.8.

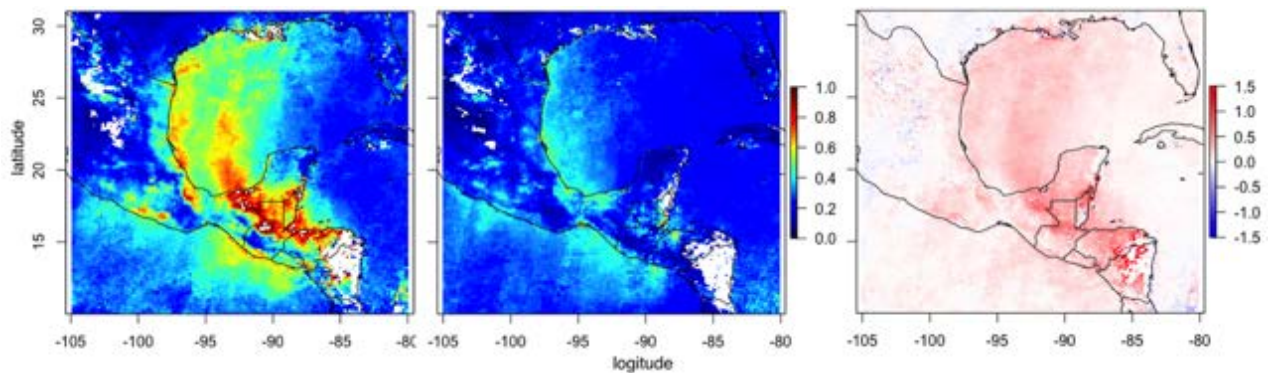


Figure 26. MODIS AOD observations from Terra satellite for the fire-impact days (left), clean-Gulf days (middle), and the difference between fire-impact days and clean-Gulf days (right). The sampling period is for April and May from 2002 to 2015.

5. Conclusion

The first part of the project identified and analyzed the days and occurrence statistics of three types of high ozone events (exceedance, top 15% peak ozone, and top 15% background ozone) and five types of meteorological events (heat wave, stagnation, thunderstorm, cold front, and post front) during the ozone season (April - October) of 2000 – 2015. Changes in peak ozone and background ozone distribution for each type of events were compared to understand and quantify their respective effects on background ozone, peak ozone, and the relative

contribution of background ozone to peak ozone at HGB. Heat wave was excluded from further analyses because of its extremely unevenly distribution.

The effect of each type of meteorological events on peak and background ozone is ranked by the change in median ozone of the event days as compared to the days with those events excluded (referred to as non-event days). Using this method, the ranking of meteorological events based on their effects on HGB peak ozone is: stagnation > post front > cold front > thunderstorm, and the ranking based on background ozone effects is: post front > cold front > stagnation > thunderstorm. Among the events analyzed in the project, only thunderstorm shows a decreasing effect on both peak and background ozone; other meteorological events are all associated with higher levels of peak and background ozone.

Stagnation is associated with increasing the median of HGB peak ozone by 26 ppbv and background ozone by 16 ppbv. Its overall co-occurrence rate with high ozone events is the highest than other meteorological events. Cold front and post front are interconnected events. Both enhance peak ozone and background ozone over the HGB area, with the latter effect being larger. The background ozone contribution during cold front and post front days are even higher than that during exceedance days. Since post front days have higher temperatures than cold front days, the associated enhancement on peak ozone and background ozone are also higher than cold front days. They co-occurred with about 15% of high ozone days.

Thunderstorm shows a decreasing effect on HGB ozone, with an 11 ppbv reduction for median peak ozone and 10 ppbv reduction for median background ozone. However, because of its frequent occurrences, thunderstorm overlaps with about 20% of high ozone days. Average background contribution during thunderstorm days is the only case that is lower than the all data set.

The hypothetical, adjusted exceedance test indicates the more important role that background ozone plays in causing ozone exceedances at HGB than local ozone. About 62% exceedance days would have been avoided over the study period if background ozone had

been reduced by 30%. Only 40% exceedance days would have been avoided if the same fractional reduction were assumed for local ozone.

In the second part of the project, we identified the impact of Central American fires on HGB background ozone for April and May from 2000 to 2015 by using back trajectory analysis and GEOS-Chem model simulations. According to the back trajectory method, the Central America fires led to an average ozone enhancement of 5.67 ± 1.00 ppbv at HGB during the study period. With the GEOS-Chem passive tracer simulation, the fire-impact days were identified by selecting the days with simulated Mexico tracer at HGB exceeding 85-percentile and burnt area over Central America exceeds 70-percentile. The GEOS-Chem-based fire-impact days were found to lead to an average ozone enhancement of 8.8 ± 1.6 ppbv at HGB for the period of April and May from 2002 to 2015. The fire-on and fire-off GEOS-Chem sensitivity simulations with full chemistry showed qualitatively consistent results of ozone enhancement at HGB. Both MOPITT and MODIS satellite instruments detect significant enhancements of CO and AOD, respectively, along the transport route from Central America fires to HGB during those identified fire-impact days. This observational evidence supports the validity of the fire-impact days derived from the project. Thus, this study has demonstrated and quantified the impact of Central American fires on HGB background ozone in an integrated perspective of satellite observations, ground measurements, and modeling.

6. Recommendation for Future Work

The present project has investigated the effects of a number of meteorological events of importance to Texas on peak and background ozone distributions at HGB. Those effects were quantified in a statistically mean sense by examining the changes in the mode of ozone distributions associated with each type of events. While this statistical approach is powerful to establish the significance and quantify the expected 'mean' magnitude of ozone changes, it cannot capture the full range of those changes, including their seasonal and interannual

variations, especially at the high tails of ozone distributions which may be more important for air quality management perspective than the mean effects. More in-depth analysis is thus needed in the future to focus on the 'tail' portion of ozone distributions and understand how this portion would be effected by meteorological conditions. This can be conducted by selectively investigating the cases at the tails and understanding how those tail cases have changed with time in response to changing emissions and meteorology through modeling and observational analysis.

There is also a need to develop an improved understanding of the physical and chemical mechanisms by which meteorological events increase peak ozone and background ozone at HGB and how those mechanisms may differ between peak ozone and background ozone. Are the associated ozone changes predominantly caused by transport of different air masses to HGB, or by meteorology-induced changes in chemistry and deposition of ozone and its precursors, or a cocktail of all those processes? Why do peak ozone and background ozone show different responses to the same type of meteorological events or factors? Answers to those questions will be valuable to guide pollution control strategies towards mitigating ozone enhancements driven primarily by meteorological conditions. For example, stagnation is found to have the largest effect of increasing both peak ozone and background ozone at HGB and also associate with the highest numbers of exceedance days. It is important to understand how high ozone is associated with both the transport of high background into HGB and stagnant wind conditions. Addressing the physical and chemical mechanisms would require attribution analysis using well-defined modeling experiments in conjunction with careful interpretation of observations.

With regard to Central American fires, we estimated that their mean effects on HGB ozone span a range of 5 and 9 ppbv during the study period (2000-2015). Given such a large impact, we recommend to conduct more case studies of the transport events of Central American fire plumes to Texas in the future in order to improve upon the estimate of the 'climatological' mean effects derived from the present report. Such case studies would require 3-D chemical transport

modeling with full representation of ozone chemistry. Because of the time and computational limitation of the present project, we only conducted two months of full chemistry simulations of fire-on and fire-off experiments using the GEOS-Chem model. Those modeling experiments show large variability between fire episodes in terms of their ozone effects at HGB and other parts of Texas. This variability warrants more future work to quantify its range, understand its linkage with large-scale transport patterns and fire source emissions, and the implications for ozone in Texas.

Finally, we recommend similar analysis to be conducted for other cities in the State of Texas that experience high ozone conditions, such as the Dallas-Fort Worth metropolitan area and San Antonio, to quantify the impacts of meteorological events and Central American fires on their ozone levels and to understand the extent to which those impacts would differ from HGB.

7. References

- Berlin, S. R., Langford, A. O., Estes, M., Dong, M., & Parrish, D. D. (2013). Magnitude, decadal changes, and impact of regional background ozone transported into the greater Houston, Texas, Area. *Environmental science & technology*, 47(24), 13985-13992.
- Kemball-Cook, S., Pavlovic, T., Johnson, J., Parker, L., Rasmussen, D. J., Zagunis, J., ... & Yarwood, G. (2014). Analysis of Wildfire Impacts on High Ozone Days in Houston, Beaumont, and Dallas-Fort Worth in 2012 and 2013. Final Report: Work Order, 582-11.
- McDonald-Buller, E., Y. Kimura, C. Wiedinmyer, C. Emery, Z. Liu, and G. Yarwood, (2015), Targeted Improvements in the Fire INventory from NCAR (FINN) model for Texas air quality planning, Prepared for the Texas Air Quality Research Project.
- McDonald, B. C., Dallmann, T. R., Martin, E. W., & Harley, R. A. (2012). Long - term trends in nitrogen oxide emissions from motor vehicles at national, state, and air basin scales. *Journal of Geophysical Research: Atmospheres*, 117(D21).
- Morris, G. A., Hersey, S., Thompson, A. M., Pawson, S., Nielsen, J. E., Colarco, P. R., ... & Johnson, B. J. (2006). Alaskan and Canadian forest fires exacerbate ozone pollution over Houston, Texas, on 19 and 20 July 2004. *Journal of Geophysical Research: Atmospheres*, 111(D24).

- Saide, P. E., Spak, S. N., Pierce, R. B., Otkin, J. A., Schaack, T. K., Heidinger, A. K., ... & Carmichael, G. R. (2015). Central American biomass burning smoke can increase tornado severity in the US. *Geophysical research letters*, 42(3), 956-965.
- Saide, P. E., Thompson, G., Eidhammer, T., Silva, A. M., Pierce, R. B., & Carmichael, G. R. (2016). Assessment of biomass burning smoke influence on environmental conditions for multiyear tornado outbreaks by combining aerosol - aware microphysics and fire emission constraints. *Journal of Geophysical Research: Atmospheres*, 121(17).
- Texas Commission on Environmental Quality (TCEQ). (2012). Houston-Galveston-Brazoria: Current attainment status; retrieved on November 16, 2014 from <http://www.tceq.texas.gov/airquality/sip/hgb/hgb-status>.
- Wang, J., Christopher, S. A., Nair, U. S., Reid, J. S., Prins, E. M., Szykman, J., & Hand, J. L. (2006). Mesoscale modeling of Central American smoke transport to the United States: 1. Top-down assessment of emission strength and diurnal variation impacts. *Journal of Geophysical Research: Atmospheres*, 111(D5).
- Wang, J., Van den Heever, S. C., & Reid, J. S. (2009). A conceptual model for the link between Central American biomass burning aerosols and severe weather over the south central United States. *Environmental Research Letters*, 4(1), 015003
- Wiedinmyer, C., Akagi, S. K., Yokelson, R. J., Emmons, L. K., Al-Saadi, J. A., Orlando, J. J., & Soja, A. J. (2011). The Fire INventory from NCAR (FINN): a high resolution global model to estimate the emissions from open burning. *Geoscientific Model Development*, 4(3), 625.
- Worden, H. M., Deeter, M. N., Edwards, D. P., Gille, J. C., Drummond, J. R., & Nédélec, P. (2010). Observations of near - surface carbon monoxide from space using MOPITT multispectral retrievals. *Journal of Geophysical Research: Atmospheres*, 115(D18).